Granular Matter (2021) 23:73
https://doi.org/10.1007/s10035-021-01134-1

ORIGINAL PAPER

Flow resistance in the transition from dense to dilute granular-fluid flows

D. Song[1,2,3] · G. G. D. Zhou[1,2,4] · Q. Chen[1,2]

Received: 9 February 2021 / Accepted: 21 June 2021

Abstract
Substantial research work has been focusing on the flow resistance of dense granular-fluid geophysical flows, e.g., debris flows. However, the mechanism of flow resistance as the dense debris flows transition to the dilute debris flow range (volumetric solid concentration 60% to 40%) remains an unsolved problem. Based on the accurate measurements of normal/shear stresses and pore fluid pressure at the flume base, we analyze the flow resistance of a series of controlled debris flow model tests, covering the flow regime from friction dominated to viscous/collisional dominated. We find that the flow resistance, excluding the Coulomb frictional component, can be well described by a visco-collisional scaling relationship. The solid–fluid interaction in the dilute range would facilitate a quick rebalance against the gravity driven force in the transient flow condition. Finally, a heuristic model is proposed to unify the flow resistance for dense and dilute debris flows.

Keywords Granular-fluid flow · Debris flow · Flow resistance · Visco-collisional scaling · Coulomb friction

1 Introduction

The landslide driving forces under gravity are mainly counterbalanced by the resistance at the bed. Basal resistance plays a key role in landslide dynamic evolution [1–3] and deposition morphology [4]. The underlying mechanisms for basal resistance are complicated and might not be unique for one specific landslide. In recent years, thermal effect [5, 6], velocity and material dependency [7, 8], and matric suction [9] have been recognized as mechanisms affecting the basal resistance of debris avalanches. Debris flows are water saturated granular-fluid mixtures with volumetric solid concentration higher than 40%. The solid–fluid interaction, *i.e.*, viscous effect, grain friction and collision, as well as the induced changes in solid concentration and pore pressure, fundamentally govern the evolution of basal and internal resistance [10–14].

We summarize different flow resistance models with their underlining physical mechanisms under varying flow regimes (dry, two-phase, viscous, collisional, and turbulent, etc.) in Table 1. Most of the models recognized the contribution of Coulomb friction and other additional effects to the flow resistance. The physics researchers [15–17] would combine Coulomb friction and other effects (particle collision or/and fluid viscous drag) into one single term. While the others [18–20] would regard the flow resistance as a simple superposition of both Coulomb friction and other effects (collision, turbulence, etc.).

Regardless of the additional viscous and collisional components of flow resistance, the resistance of dense debris flow is dominated by the particle normal stress σ_n (effective stress in soil mechanics, defined as the difference between total normal stress σ_{tot} and pore pressure p, [14, 23]) which in form obeys the Coulomb friction law [24]. Yet, as dense debris flows (typical solid concentration around 60%) transition to moderate and dilute debris flows (with solid concentration still higher than 40%, [12]), the particle normal stress diminishes. The dominant mechanisms behind the shear resistance in the dilute range are still not clearly understood [25]. The flow resistance may be purely due to viscous effect

✉ G. G. D. Zhou
gordon@imde.ac.cn

1 Institute of Mountain Hazards and Environment, Chinese Academy of Sciences, Chengdu, China

2 University of Chinese Academy of Sciences, Beijing, China

3 School of River and Ocean Engineering, Chongqing Jiaotong University, Chongqing, China

4 China–Pakistan Joint Research Center on Earth Sciences, CAS-HEC, Islamabad, Pakistan

Published online: 24 July 2021

Table 1 Flow resistance models under varying flow regimes

Flow regime	Flow resistance model	Key parameters	Physical mechanisms	Reference
Single phase; colloidal flow	1 $\tau = \tau_y + k\dot{\gamma}^n$	τ: flow resistance (shear stress); $\dot{\gamma}$: shear rate; τ_y: yield stress; k & n: constitutive parameters	Shear-thinning ($n<1$) or shear-thickening ($n>1$) with yield stress	Herschel–Bulkley model Acheson [21]
Dense granular flow	2 $\tau = \mu(I)\sigma_n$	μ: dynamic friction coefficient; σ_n: particle normal stress; I: inertial number	Coulomb friction with collision induced resistance	GDR MiDi [15]
	3 $\tau = \mu\sigma_n + \mu'(I)\dot{\gamma}$	μ': dynamic friction coefficient for collisional effect	Coulomb friction with collision induced resistance	Ancey and Evesque [18]
	4 $\tau = \mu\sigma_n + c\dot{\gamma}^2$	c: constant up to particle normal stress $\sigma_n \sim 10^4$ Pa	Coulomb friction with collision induced resistance	Rauter et al. [19]
Dense granular-fluid flow	5 $\tau = \mu(I_v)\sigma_n$	I_v: viscous number	Coulomb friction with viscosity induced resistance	Boyer et al. [16]
	6 $\tau = \mu(K)\sigma_n$	K: mixed dimensionless number $K = I_v + \alpha I^2$	Coulomb friction with visco-collision induced resistance	Trulsson et al. [17]
Turbulent avalanche flow	7 $\tau = \mu\sigma_n + \rho g v^2/\xi$	ρ: density of flow; g: gravitational acceleration; v: flow velocity; ξ: turbulence coefficient	Coulomb friction with turbulence induced resistance	Voellmy model Bartelt et al. [20, 22]

as it is fully liquefied [12], or due to collisional forces mediated by fluid [2, 26, 27], or a combination of both.

Owing to the poor mechanistic linkage between the causes and effects in field monitoring, experimental data is needed to discriminate between different physical mechanisms. Through modelling and analysis of steady uniform submarine granular flows down an inclined plane, Cassar et al. [28] found that, for dense submarine granular flows, the role of viscous fluid is to change the time scale for a particle to rearrange into a hole (void). A Coulomb friction law with a coefficient of friction depending on the shear rate and fluid properties is proposed, which is further developed by Boyer et al. [16]. Kaitna et al. [29] directly measured the velocity profile of steady granular-fluid flows using a velocity probe (conductivity sensors) in a rotating drum. It is found that the coarse mixture composition and fines content can alter the velocity profile significantly. For the gravel-water mixtures, where the fluid effects are of minor importance, the velocity profiles are close to a Bagnoldian (inertial) or viscous scaling. The above experimental investigations focus on the dense granular-fluid flows. Research on the dilute granular-fluid flows is still rare.

This paper reports accurate measurement of shear resistance obtained synchronously with the normal stress and pore fluid pressure at the flume base of a series of controlled granular-fluid flow model tests. To focus on the transition from dense to dilute debris flows, the solid concentration is varied. The origin of shear resistance in dilute debris flows is elaborated and a heuristic model unifying the flow resistance of dense and dilute debris flows is proposed.

2 Experimental setup and material

2.1 2.1 Model setup and instrumentation

The experimental flume consists of a container at the upstream and a linear transportation zone (Fig. 1a). The width of flume is 300 mm. The bed is roughened by gluing 0.6 mm diameter glass beads which is also used as the solid phase of the modelled debris flows. The inclination of the flume is kept constant at 20° in all the tests.

The normal and shear stresses are measured using a basal sensing module (triaxial load cell, LH-SZ-02, 50 N, ± 0.1% BSL, see Fig. 1b, c) at the flume base, located 1700 mm downstream of the container. The normal and shear stresses are calculated based on the measured force and the surface area of force plate. The measured normal and shear stresses reflect the reaction to all on-going shear processes (frictional, collisional, and viscous) integrated over the depth of flow. Different from the normal stress, the reliable measurement of shear stress remains a technical challenge which hinders further understanding of the development of shear resistance under transient flow condition. On one hand, the gap between the base plate and force plate (Fig. 1b) should be filled up to prevent jamming caused by the hard particles. On the other hand, the filling material must be soft enough as to provide negligible stiffness in the tangential direction [23]. During calibration of the basal sensing module, serious creeping effect was found for the soft gap-filling material, which

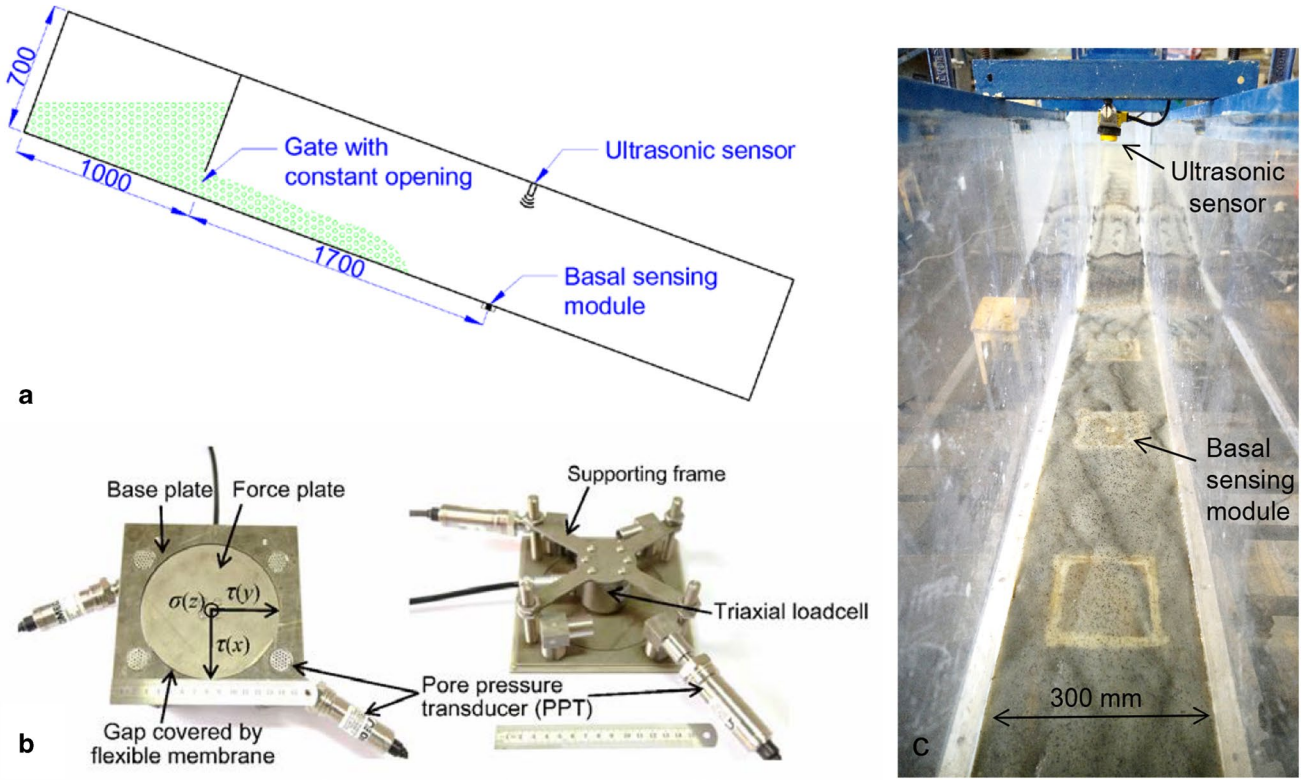

Fig. 1 **a** Flume setup and instrumentation. All units are in mm. **b** Basal sensing module for measurement of normal/shear stresses and pore pressure. Left: up side; right: bottom side. Gap between the base plate and force plate is covered by flexible membrane (coating layer) to prevent particles falling into. **c** Internal structure of the flume (with debris deposition on the flume bed)

would cause additional resistance on the dynamic loading and strong hysteresis on the cyclic loading. We solve this problem by covering the gap between the base plate and force plate with a very thin coating layer (Fig. 1b) with negligible stiffness. Separate calibration is conducted for the one with coating layer on the gap and the one without any coating layer. The calibration results show that there is less than 5% difference in the force coefficient (and thus the additional stiffness), denoting reliable measurement of the shear stress.

Pore fluid pressure is recorded using pore pressure transducer (PPT, OMEGA PX409-001G5V, 6.9 kPa, $\pm 0.08\%$ BSL, Fig. 1b). The open end of the PPT is covered by a 0.4 mm steel mesh, which isolates the pressure induced by the solid phase. Flow depth is measured using an ultrasonic sensor (BANNER U-GAGE T30UXUA, 0.1–1.0 m, resolution 0.1% of distance) right above the basal sensing module (Fig. 1c). A high speed camera (PHONTRON FASTCAM Mini WX50) with resolution of 1280×1024 pixels with combination of LED light illumination is set aside the flume. The frontal velocity is calculated based on the travel time of the flow front along a 0.15 m distance. Sampling rate of the whole data acquisition system is 500 Hz.

2.2 Test program and material

In terms of material properties, natural debris flows are characterized by a wide grain size distribution and a non-Newtonian fluid rheology resulting from the inclusion of fine content into fluid phase. This study simplifies real debris flows as a suspension of mono-sized glass beads (0.6 mm, 2540 kg/m^3 particle density) and Newtonian fluid (glycerol-water mixture). On one hand, without enough understanding on a simplified "debris flow", it is pessimistic to reveal the complicated mechanisms of natural debris flows. On the other hand, the simplification of debris flow facilitates the deterministic analysis of stress decomposition. The mono-sized solid phase bypasses the problems of determining the representative grain size for the calculation of collisional stress [2] and the mediation of shear resistance by grain-size segregation [30, 31]. Compared with well-graded natural debris material, mono-sized particles occupy a larger bulk volume and are featured with less compressibility. A dynamic friction coefficient of 0.56 is adopted for glass beads. The use of a Newtonian fluid circumvents the difficulties related to finding a threshold particle diameter and appropriate viscosity for the slurry phase.

To investigate the dominant mechanisms responsible for the shear resistance in the transition from dense to moderate and dilute debris flows, solid concentration is varied among 60%, 50%, and 40%. Fluid viscosity is varied among 0.1 Pa·s, 0.05 Pa·s, 0.01 Pa·s, and 0.001 Pa·s (viscosity of water) to cover the typical range of real debris flow viscosity [32]. Changing the viscosity also helps to elucidate the contribution of fluid viscous effect to the shear resistance. The test program used in this study is summarized in Table 2.

In the container, the granular-fluid suspensions remain well-mixed by using a helical mixer. Rather than creating a steady state flow condition (i.e., constant flow depth and hydrostatic pore pressure) which is not feasible for the physical modelling, this study releases the debris material at a constant gate opening. By this approach, we investigate if the transient flows regain balance from the initial release through development of flow resistance.

3 Results and interpretation

3.1 3.1 Measured normal/shear stresses and pore pressures

Figure 2 shows the measured normal/shear stresses and pore pressures at the flume base for tests with 0.1 Pa·s fluid viscosity. Time zero denotes the release of debris material from the container. To remove the high-frequency fluctuations, the pore pressure data is processed using the moving average method with an interval of 0.02 s. The flows with high solid concentration (60%) are characterized with low frontal velocities (e.g., 0.13 m/s for test 60–100), reaching a steady discharge for more than 10 s. The measured normal stress, shear stress, pore fluid pressure, and flow depth are all steady within this period (Fig. 2a1,a2). While the moderate and low solid concentration (50% and 40%) flows are characterized with relatively high frontal velocities (e.g., 2.63 m/s for test 50–100 and 3.13 m/s for test 40–100). The discharge and measured parameters vary quickly with time (Fig. 2b1–c2).

Previous experimental and numerical analyses usually assume that granular-fluid flows are in a steady state condition [28]. Under this assumption, the total normal stress σ_{tot} equals the bed-normal component $\rho gh\cos\theta$ imposed by the bulk flow, and the shear stress τ equals the bed-tangential component $\rho gh\sin\theta$, where ρ is bulk density of flow (kg/m^3, Table 2), g is gravitational acceleration (9.81 m/s^2), h is flow depth (m), and θ is slope inclination. In this study, the calculated normal stress $\rho gh\cos\theta$ is close to the measured normal stress for all the tests, corroborating the accuracy in normal stress and flow depth measurement. The measured shear stress for test 60–100 matches the driving force (calculated shear stress) $\rho gh\sin\theta$ (Fig. 2a2). However, for test 50–100, the shear stress curve is characterized by a sharp increase in shear resistance which may be caused by the turbulence in the thin flow front. Right after the flow front has passed, the driving force (calculated shear stress) coincides with that of the measured stress (Fig. 2b2). This means that the developed flow resistance is in balance with that of gravity driven force. Further decreasing the solid concentration to 40%, driving force $\rho gh\sin\theta$ is higher than the measured value, implying that the flow is accelerating (Fig. 2c2). The trend in tests with 0.01 Pa·s viscosity (Fig. 3) is similar with those of 0.01 Pa·s viscosity (Fig. 2).

For dense granular-fluid flows, the friction induced by the particle normal stress σ_n (effective stress in soil

Table 2 Test program and relevant flow regimes. Test ID "60–100" denotes test with 0.60 solid concentration and 0.1 Pas viscosity (100 times of water viscosity)

Test ID	Solid concentration	Fluid density ρ_f (kg/m^3)	Bulk density ρ (kg/m^3)	Fluid viscosity η (Pa·s)	Equivalent viscosity η_{eq} (Pa·s)	Stokes number St	Bagnold number N_B	Regime based on Courrech du Pont et al. [10]
60–100	0.6	1220	2010.6	0.1	21.6	0.04	0.07	Viscous
60–50		1205	2004.2	0.05	8.6	0.21	0.32	Viscous
60–10		1145	1979.6	0.01	2.0	2.39	3.58	Viscous
60–1		1000	1924.0	0.001	1.2	39.01	58.51	Inertial
50–100	0.5	1220	1878.2	0.1	3.5	0.77	0.77	Viscous
50–50		1205	1870.2	0.05	3.1	1.45	1.45	Viscous
50–10		1145	1839.4	0.01	1.1	12.78	12.78	Inertial
50–1		1000	1770.0	0.001	0.6	196.33	196.33	Inertial
40–100	0.4	1220	1745.8	0.1	1.9	0.88	0.59	Viscous
40–50		1205	1736.2	0.05	1.7	1.78	1.19	Viscous
40–10		1145	1699.2	0.01	0.7	13.37	8.91	Inertial
40–1		1000	1616.0	0.001	–	–	–	Solid–fluid segregation

Due to the apparent solid–fluid segregation, test 40–1 is excluded from the calculation of flow regime

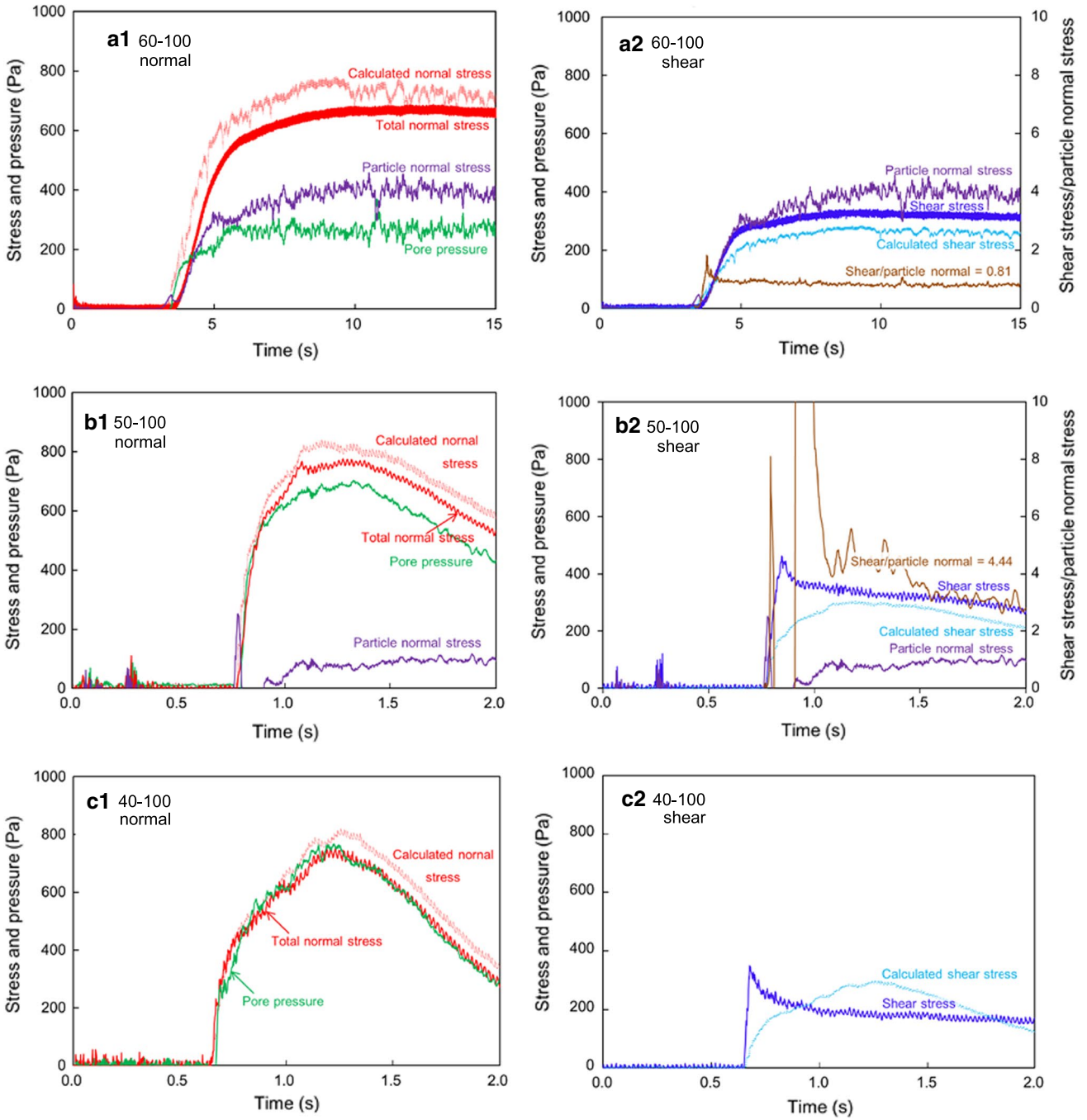

Fig. 2 Measured and calculated stresses of tests with viscosity of 0.1 Pa·s: **a1**–**a2** Normal and shear stresses of test 60–100 (60% solid concentration and 0.1 Pa·s viscosity). **b1**–**b2** Normal and shear stresses of test 50–100. **c1**–**c2** Normal and shear stresses of test 40–100

mechanics, the difference between total normal stress σ_{tot} and pore pressure p) is regarded as the main source of shear resistance, and the experimental results support this. In tests 60–100 and 60–10, the ratio between measured shear and particle normal stresses, $\tau/\sigma_n = 0.81$ and 0.68, are slightly higher than the dynamic friction coefficient of glass beads $\mu = 0.56$ (Figs. 2a2 and 3a2). The random packing concentration of mono-sized spherical particles is around 60%. As the solid concentration reduces to 50%, most particles lose contact with each other. For test 50–100, pore pressure reaches up to 90% of the total normal stress, implying that the flow is almost liquefied and the granular structure is largely supported by the interstitial pore fluid (Fig. 2b1). The ratio between measured shear and particle normal stresses (averaged over the period of steady particle normal stress), $\tau/\sigma_n = 4.44 >> 0.56$, could

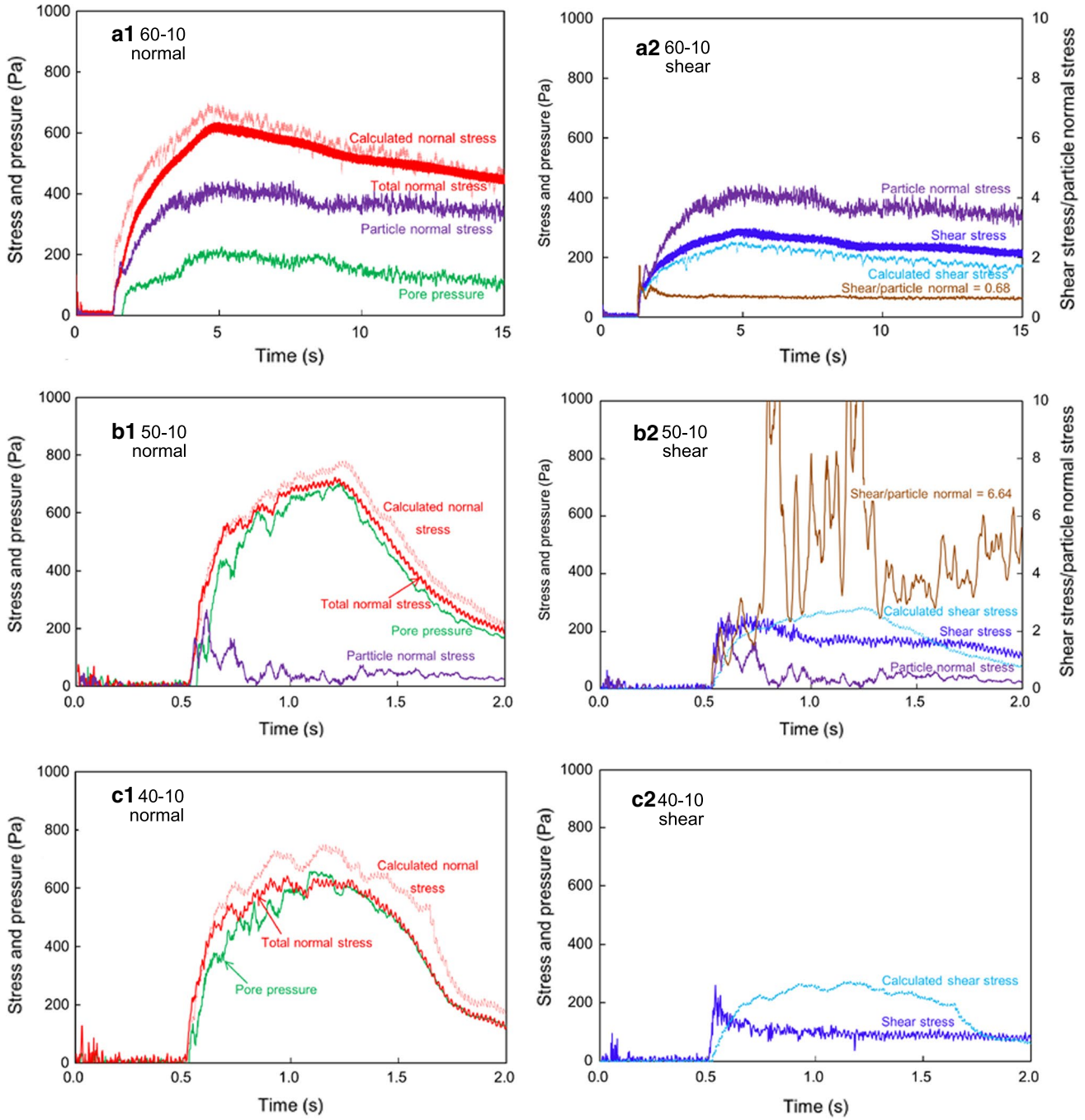

Fig. 3 Measured and calculated stresses of tests with viscosity of 0.01 Pa·s: **a1**–**a2** Normal and shear stresses of test 60–10 (60% solid concentration and 0.01 Pa·s viscosity). **b1**–**b2** Normal and shear stresses of test 50–10. **c1**–**c2** Normal and shear stresses of test 40–10

not be therefore attributed to the particle normal stress (Fig. 2b2). This ratio is much higher than that predicted by the rheology of dense granular flows and debris flows (around unity, [16, 17]). This is more so for test 40–100, where the flow is completely liquefied, resulting in an infinite ratio, indicating the poor applicability of the dense granular flow rheology in the dilute debris flow range. It was previously suggested that the source of shear resistance for dilute debris flows may come from grain collision [33, 34] or viscous effect [12]. Both mechanisms will be further investigated in the following sections.

3.2 3.2 Flow regimes

We adopt the approach proposed by Courrech du Pont et al. [10] in distinguishing the relative dominance of viscous or inertial (grain collision) effects. There exists three regimes—free fall, inertial limit, and viscous limit—for granular flows in fluids. Each regime is characterized by the Stokes number and the density ratio. The Stokes number St defines the ratio of the grain inertia over the fluid viscous effect:

$$St = \frac{\rho_s \dot{\gamma} \delta^2}{\eta} \tag{1}$$

The density ratio is expressed as follows:

$$r = \sqrt{\frac{\rho_s}{\rho_f}} \tag{2}$$

where ρ_s and ρ_f are the densities of the solid phase and fluid phase (kg/m^3, Table 2), respectively; δ is representative particle diameter (m); η is dynamic viscosity of fluid (Pa·s); $\dot{\gamma}$ is the depth averaged shear rate (1/s); for a viscous flow profile, $\dot{\gamma} = 3v/2h$, and for Bagnoldian (inertial) flow profile, $\dot{\gamma} = 5v/3h$, where v is flow velocity (m/s) and h is flow depth (m). For the determination of shear rate, a trial and error approach is adopted. The flow regime is first assumed to be viscous, and the calculated St is verified against the viscous regime in Fig. 4; otherwise, it falls into the inertial regime (Table 2) and the St should be recalculated. In this study, the density ratio only varies from 1.44 to 1.59. A third dimensionless value, the particle Reynolds number $Re_p = St/r = 2.5$, sets the boundary between grain inertial and viscous effects. In Fig. 4, only one representative data point for each test is adopted. For steady state flows (high solid concentration), the frontal velocity and flow depth from the steady period are adopted. For transient flows (moderate and low concentration), frontal velocity and peak flow depth are adopted.

For the range of solid concentration and viscosity adopted in this study, experimental data points fall into either the fluid viscous or grain inertial regimes (Fig. 4 and Table 2). With the variation in solid concentration and fluid viscosity, the modelled flows gradually transition from one regime to another. For natural viscous debris flows, solid particles follow the trajectory of the fluid phase, which usually happen in flows with high fine content and small particles (Fig. 5a). While, substantial velocity different exists between solid and fluid phases in inertial debris flows (Fig. 5b).

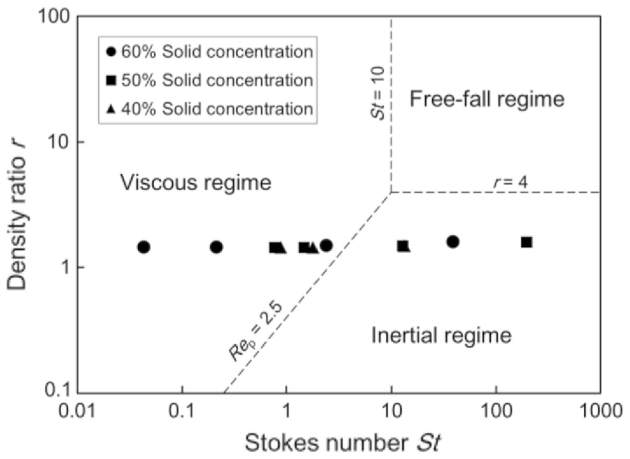

Fig. 4 Flow regimes of modelled debris flows in the (St, r) space. Thresholds of Stokes number St, density ratio r, and particle Reynolds number Re_p are from Courrech du Pont et al. [10]

3.3 3.3 Flow resistance in dense and dilute debris flows

The influence of grain collision and viscous effects on the friction coefficient ($\mu = \tau/\sigma_n$) can be unified through the mixed dimensionless number $K = I_v + \alpha I^2$ [17], with viscous number

$$I_v = \frac{\dot{\gamma}\eta}{\sigma_n} \tag{3}$$

inertial number

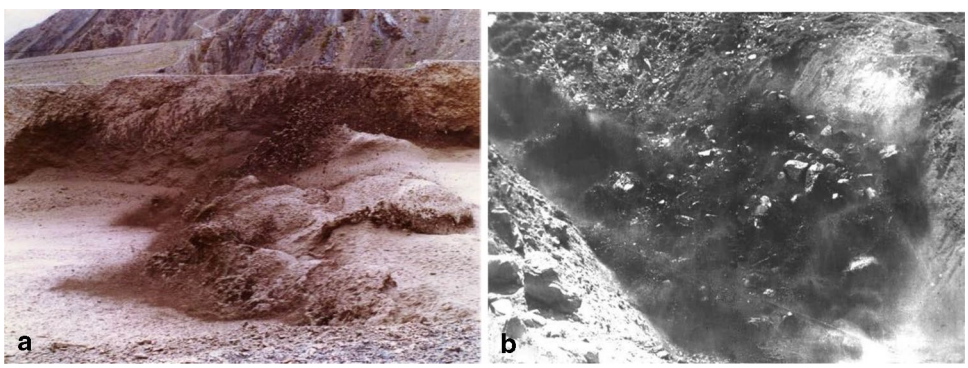

Fig. 5 **a** Typical viscous flow: debris flow front captured at DDFORS (Dongchuan Debris Flow Observation and Research Station) of Chinese Academy of Sciences. **b** Typical inertial flow: experimental debris flow in 1975 at Chemolgan test site [35]

$$I = \frac{\dot{\gamma}\delta}{\sqrt{\sigma_n/\rho_s}} \tag{4}$$

and $\alpha = 0.635$ as deduced by Trulsson et al. [17]. As can be seen in Fig. 6, μ generally increases with the increase of K. As predicted by the rheology of dense granular-fluid flows, data points for 60% flows all well collapse into one curve around unity. While Data points for 50% flows are scattered and the values of friction coefficients are much higher than that predicted by the rheology of dense granular flows (around unity). Moreover, since the 40% solid concentration flows are characterized by negligible or zero effective stress, the friction coefficient goes to infinity, indicating the poor applicability of the dense granular flow rheology in the dilute debris flow range.

Based on the granular kinetic theory, we further postulate that the shear resistance higher than the Coulomb friction originates from the collisional effects, with a mechanism different from the dense granular framework [36]. The kinetic theory for dry granular flow requires the estimation of the granular temperature T from the stress perspective or granular fluctuation energy from the energy perspective [37, 38], which is difficult to measure in physical experiments since tracking a single particle that is far from the sidewall is infeasible. Rauter et al. [19] proposed that the granular temperature can be expressed as a function of the square of shear rate, $T = f(\dot{\gamma}^2)$. The total flow resistance can be expressed based on an extended kinetic theory which considers the Coulomb frictional contribution (if present) of the flow:

$$\tau = \mu\sigma_n + c\dot{\gamma}^2 \tag{5}$$

where c is approximated as a constant up to a particle normal stress σ_n of 10^4 Pa [19]. The term $c\dot{\gamma}^2$ bears a similar physical meaning as with the Bagnold dispersive stress $\rho_s\dot{\gamma}^2\delta^2$. For the granular-fluid flows in this study, we plot the Bagnold stress $\rho_s\dot{\gamma}^2\delta^2$ against the flow resistance excluding the Coulomb frictional contribution τ-τ_C, where $\tau_C = \mu\sigma_n$ is the calculated shear component from the particle normal stress σ_n and $\mu = 0.56$ is dynamic friction coefficient of solid phase. Note both the Coulomb friction and collisional/viscous resistance could change according to the flow regime. In order to analyze the collisional/viscous resistance, we would preliminarily fix the dynamic friction coefficient μ as a constant. As shown in Fig. 7a, nevertheless, the flow resistance τ–τ_C decreases with increasing Bagnold stress. Although scattered in a wide range, there is high correlation between the shear resistance and fluid viscosity, as shear resistance decreases proportionally with the deceasing fluid viscosity (Fig. 7a). This implies that both the viscous and collisional effects contribute to the flow resistance τ–τ_C.

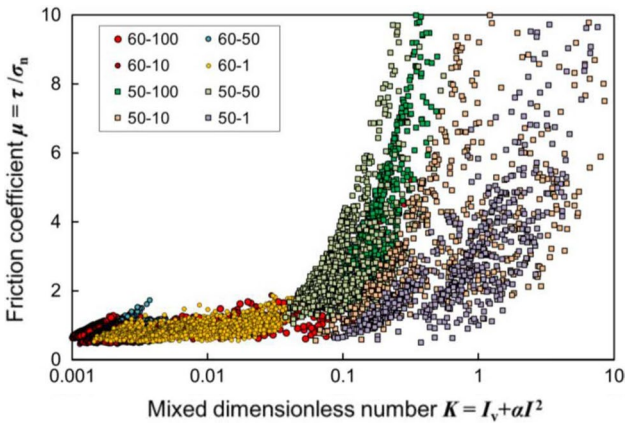

Fig. 6 Relationship between friction coefficient μ and the mixed dimensionless number K

The Bagnold number is further adopted to quantify the contribution of solid–fluid interaction to shear resistance. Bagnold number N_B represents the relative importance between collisional and viscous effects [33, 39]:

$$N_B = \left[\frac{\upsilon_s}{1-\upsilon_s}\right]\frac{\rho_s\dot{\gamma}\delta^2}{\eta} \tag{6}$$

where υ_s is volumetric solid concentration; ρ_s is density of solid phase (kg/m^3); $\dot{\gamma}$ is depth averaged shear rate (1/s); δ is representative particle diameter (m); and η is dynamic viscosity of fluid (Pa·s). The dimensionless shear stress $(\tau$-$\tau_C)\rho_s\delta^2/(\lambda\eta^2)$, proposed by Bagnold [39], is adopted to eliminate the influence of fluid viscosity η, where $\lambda = \upsilon_s/(1$-$\upsilon_s)$. Figure 7b shows the dimensionless shear stress (excluding the Coulomb friction component) over the full range of Bagnold number in logarithmic scale. Each experimental data set collapses into one cluster, and the 15 cluster of data points of various viscosity and collisional stress now collapse into a single curve. Note that Bagnold number only differs from the Stokes number by a constant $\lambda = \upsilon_s/(1-\upsilon_s)$. When the same data points are plotted against the Stokes number, they do not perfectly collapse, reflecting the influence of solid concentration υ_s, and hence the state of dilution on the solid–fluid interaction and flow resistance.

4 Discussion

Special concern is raised on whether the measured parameters of unsteady flows could be used to extract the law of flow resistance. Especially, for experimental study without basal shear stress measurement, a steady state has to be reached, so that the basal resistance gets balanced by the gravity component along the slope (see Cassar et al. [28]). On the contrary, the measured basal shear stresses in this study is an instant reflection of the basal resistance and flow regime, no matter the flow is steady or not. Thus, a lumped

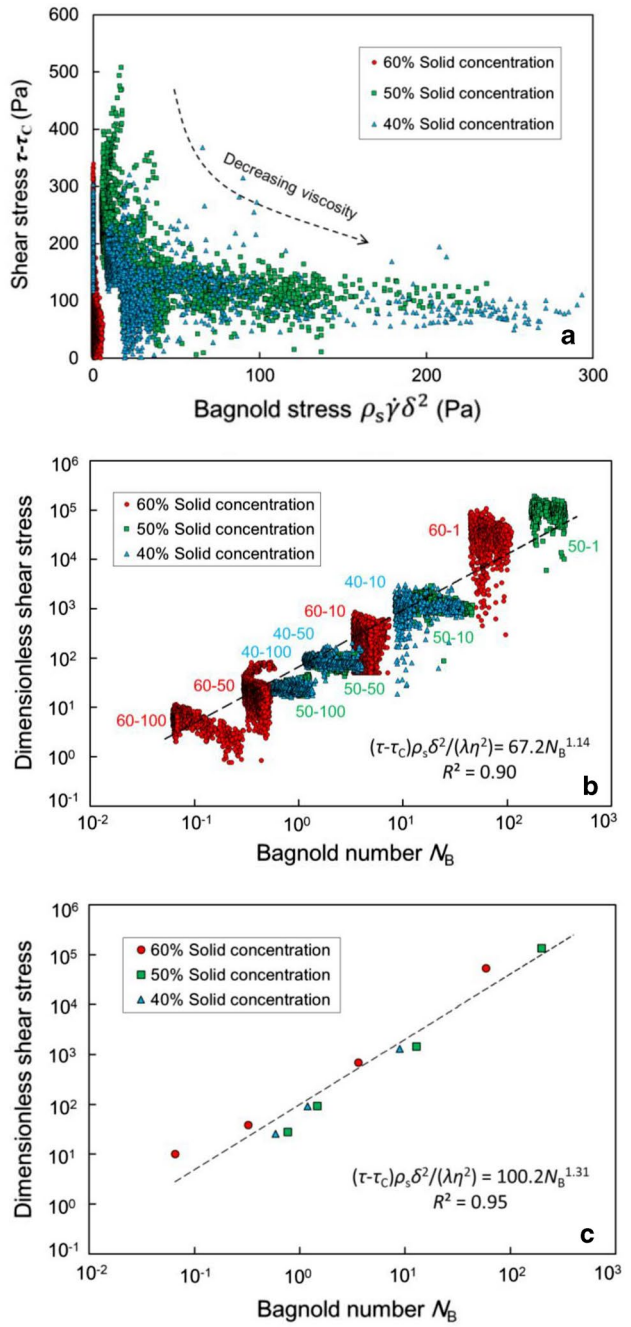

Fig. 7 **a** Relationship between the Bagnold collisional stress $\rho_s\dot{\gamma}^2\delta^2$ and shear resistance $\tau-\tau_C$ excluding the Coulomb frictional component. **b** Collapse of data points into a single curve after adopting the Bagnold number N_B. **c** Plot of **b** using the representative data points

analysis, without consideration of the temporal variation of the unsteady flow, provides more realistic data for the basal resistance. For comparison, plot with representative data points is also shown in Fig. 7c. From Fig. 7b and c, although with slightly different fitting values, it is apparent that the law of basal resistance is not affected by the unsteady property of debris flow.

Half of the tests fall into the viscous flow regime (Fig. 4), which means that fluid viscous drag may be the major component of flow resistance. Take test 50–100 as an example, the particle friction in test 50–100 is already pretty weak (Fig. 2b2). However, the back calculated equivalent viscosity $\eta_{eq} = (\tau - \tau_C)/\dot{\gamma}$ for the viscous flow cases are all much higher than the viscosity of pure fluid η (see Table 2). In fact, the macro-viscous regime named by Bagnold [39] implicitly includes the effect of solid particles on the viscous effect. On the other hand, for the flows in the collisional regime, for tests 50–10 and 50–1, the Bagnold collisional stress is still negatively correlated to the shear resistance τ-τ_C (Fig. 7a), denoting the nontrivial effect of pore fluid in the collisional regime. The complex visco-collisional interaction can be well described by the Bagnold scaling (Fig. 7b).

The experimental finding presented here also has implications to numerical simulation [40, 41] of debris flows and relevant geophysical flows. As dense debris flows reduce to dilute debris flows, the particle normal stress diminishes and the flow becomes liquefied. In many cases, numerical models which consider frictional and pure fluid viscous resistances, degrade to viscous fluid models [12]. However, the experimental flows in this study are observed to display balance against gravity-driven forces through visco-collisional effects. Numerical models aiming to describe the wide spectrum of geophysical flows, including dense-dilute debris flows, debris floods, etc., should take visco-collisional interaction into account.

The rheological model for dense granular-fluid flows [16, 17] only applies to the 60% solid concentration flows, where the friction effect dominates (reflected by the substantial particle normal stress in Figs. 2a1 and 3a1); while viscous and collisional effects remain secondary contributions to the flow resistance. As the grain contact friction (particle normal stress) vanishes with the decrease of solid concentration, the viscous/collisional stresses take over to become the main mechanisms of solid–fluid interaction. A flow resistance model that can cover a wide spectrum of flow regimes thus should reflect the friction-dominated effect for dense debris flows and visco-collisional effect which is dominant in dilute debris flows. As inspired by Rauter et al. [19], who extended the kinetic theory to a function of both frictional and collisional effects (Eq. 3), we propose that the flow resistance expression for granular-fluid flows should include the contribution of both frictional (if present) and visco-collisional forces. Based on the experimental findings featured in Fig. 7b and c, a unified heuristic model of the shear resistance for dense and dilute debris flows can be expressed as follows:

$$\tau = \mu\sigma_n + a\frac{\lambda\eta^2}{\rho_s\delta^2}N_B^b \tag{7}$$

where a and b are dimensionless constants; $a = 67.2$ and $b = 1.14$ based on Fig. 7b. The value of b lies within the

range of viscous shear stress ($\dot{\gamma}^b\eta$ with $b=1$) and Bagnold dispersive stress ($\rho_s\dot{\gamma}^b\hat{\delta}^2$ with $b=2$), implying the joint contribution of viscous and collisional effects to the shear resistance.

The Bagnold number can be further substituted into Eq. (7) and the depth averaged shear rate $\dot{\gamma}$ can be estimated from the flow velocity v and depth h. Equation (7) can finally be rewritten as follows:

$$\tau = \mu\sigma_n + \chi\lambda^{b+1}\beta^b\left(\frac{v}{h}\right)^b \tag{8}$$

where χ is a constant related with material properties (particle density, particle diameter, and fluid viscosity); $\lambda = \upsilon_s/(1\text{-}\upsilon_s)$ is related to the solid concentration υ_s; β is a factor for velocity profile, $\beta=3/2$ for viscous profile, $\beta=5/3$ for Bagnoldian (inertial) profile. This expression is similar to the Voellmy rheological model (Table 1) where additional flow resistance comes from the square of the velocity v^2. Rather than the turbulent effects in the Voellmy model, the additional flow resistance in Eq. (8) originates from the visco-collisional effect of solid–fluid interaction. Another key difference of Eq. (8) from the Voellmy model is the inverse dependency on the flow height h, and this would lower the modelled stress value [19]. Flows with thicker flow depth would result in lower stress value, and this in turn enhances the flow velocity and flow volume. As for water-saturated debris flows, on one hand, a thicker flow depth facilitates the maintenance of excess pore pressure by elongating the time of pore pressure dissipation [11, 13], thus reduces the particle normal stress in the first term of right hand side of Eq. (8). On the other hand, it limits the rate-dependent visco-collisional contribution to the shear resistance in the second term.

5 Conclusions

A wide spectrum of geophysical flows exist with the variation of volumetric solid concentration, from saturated dense debris flow to dilute debris flow, debris flood, and then sediment-laden flow. Current research mainly focuses on the flow behaviors (rheology) at the two sides of the spectrum. However, much are not clear about behavior for the flows in between. Based on the accurate measurements of shear stress, this study analyzes the flow resistance ranging from friction dominated to viscous/collisional dominated flows. The rheological model for dense granular-fluid flows, whose principal mechanism for shear resistance and energy dissipation is the particle normal stress, has poor applicability to dilute debris flows. Despite fully liquefied in the dilute debris flows, both the solid and fluid phases contribute to the bulk flow forces. The flow resistance excluding the Coulomb frictional component can be well described by a visco-collisional scaling relationship. As a compensating mechanism of this visco-collisional effect, the apparent flow resistance of dilute debris flows remains nontrivial. However, due to lacking of accurate measurement on the shear stress, this nontrivial flow resistance is usually incorrectly attributed to the frictional effect.

A heuristic model is further proposed to unify the flow resistance of dense and dilute debris flows. Currently, the numerical prediction for dilute debris flows would adopt the rheology of pure fluid, since the flows remain fully liquefied and no particle normal stresses (effective stress) exist. Numerical simulation with consideration of visco-collisional resistance shall see the difference in modelling landslide dynamic evolution, basal erosion, mobility, and related hazard mapping.

Acknowledgements The authors acknowledge the financial supports from the National Natural Science Foundation of China (Grant No. 41925030, 42077256, and 51809261), CAS "Light of West China" Program, and the Sichuan Science and Technology Program (Grant No. 2020YJ0002). Support from the DDFORS (Dongchuan Debris Flow Observation and Research Station) of Chinese Academy of Sciences is acknowledged.

Availability of data and materials The experimental data is available upon request to the first author (D. Song, drsong@imde.ac.cn).

Declaration

Conflict of interest The authors declare no conflicts of interest on the submitted work.

References

1. Hungr, O.: Simplified models of spreading flow of dry granular material. Can. Geotech. J. **45**(8), 1156–1168 (2008). https://doi.org/10.1139/T08-059
2. Kaitna, R., Palucis, M.C., Yohannes, B., Hill, K.M., Dietrich, W.E.: Effects of coarse grain size distribution and fine particle content on pore fluid pressure and shear behavior in experimental debris flows. J. Geophys. Res. Earth Surf. **121**(2), 415–441 (2016). https://doi.org/10.1002/2015JF003725
3. Zhou, G.G.D., Song, D., Choi, C.E., Pasuto, A., Sun, Q.C., Dai, D.F.: Surge impact behavior of granular flows: effects of water content. Landslides **15**(4), 695–709 (2018). https://doi.org/10.1007/s10346-017-0908-6
4. Haas, T., Braat, L., Leuven, J.R., Lokhorst, I.R., Kleinhans, M.G.: Effects of debris flow composition on runout, depositional mechanisms, and deposit morphology in laboratory experiments. J. Geophys. Res. Earth Surf. **120**(9), 1949–1972 (2015). https://doi.org/10.1002/2015JF003525
5. Wang, Y.F., Dong, J.J., Cheng, Q.G.: Velocity-dependent frictional weakening of large rock avalanche basal facies: Implications for rock avalanche hypermobility? J. Geophys. Res. Solid Earth **122**, 1648–1676 (2017). https://doi.org/10.1002/2016JB013624
6. Hu, W., Huang, R., McSaveney, M., Yao, L., Xu, Q., Feng, M., Zhang, X.: Superheated steam, hot CO2 and dynamic

recrystallization from frictional heat jointly lubricated a giant landslide: field and experimental evidence. Earth Planet. Sci. Lett. **510**, 85–93 (2019). https://doi.org/10.1016/j.epsl.2019.01.005
7. Lucas, A., Mangeney, A., Ampuero, J.P.: Frictional velocity-weakening in landslides on Earth and on other planetary bodies. Nat. Commun. **5**, 3417 (2014). https://doi.org/10.1038/ncomms4417
8. Scaringi, G., Hu, W., Xu, Q., Huang, R.: Shear-rate-dependent behavior of clayey bimaterial interfaces at landslide stress levels. Geophys. Res. Lett. **45**(2), 766–777 (2018). https://doi.org/10.1002/2017GL076214
9. Zhou, G.G.D., Li, S., Song, D., Choi, C.E., Chen, X.Q.: Depositional mechanisms and morphology of debris flow: physical modelling. Landslides **16**(2), 315–332 (2019). https://doi.org/10.1007/s10346-018-1095-9
10. Courrech Dupont, S., Gondret, P., Perrin, B., Rabaud, M.: Granular avalanches in fluids. Phys. Rev. Lett. **90**(4), 044301 (2003). https://doi.org/10.1103/PhysRevLett.90.044301
11. McArdell, B.W., Bartelt, P., Kowalski, J.: Field observations of basal forces and fluid pore pressure in a debris flow. Geophys. Res. Lett. (2007). https://doi.org/10.1029/2006GL029183
12. Iverson, R.M., George, D.L.: A depth-averaged debris-flow model that includes the effects of evolving dilatancy. I. Physical basis. Proc. R. Soc. Lond. Ser. A (2014). https://doi.org/10.1098/rspa.2013.0820
13. Iverson, R.M.: Scaling and design of landslide and debris-flow experiments. Geomorphology **244**, 9–20 (2015). https://doi.org/10.1016/j.geomorph.2015.02.033
14. Nagl, G., Hübl, J., Kaitna, R.: Velocity profiles and basal stresses in natural debris flows. Earth Surf. Proc. Land. **45**(8), 1764–1776 (2020). https://doi.org/10.1002/esp.4844
15. GDR MiDi: On dense granular flows. Eur. Phys. J. E **14**(4): 341–365. https://doi.org/10.1140/epje/i2003-10153-0 (2004).
16. Boyer, F., Guazzelli, É., Pouliquen, O.: Unifying suspension and granular rheology. Phys. Rev. Lett. **107**(18), 188301 (2011). https://doi.org/10.1103/PhysRevLett.107.188301
17. Trulsson, M., Andreotti, B., Claudin, P.: Transition from the viscous to inertial regime in dense suspensions. Phys. Rev. Lett. **109**(11), 118305 (2012). https://doi.org/10.1103/PhysRevLett.109.118305
18. Ancey, C., Evesque, P.: Frictional-collisional regime for granular suspension flows down an inclined channel. Phys. Rev. E **62**(6), 8349 (2000). https://doi.org/10.1103/PhysRevE.62.8349
19. Rauter, M., Fischer, J.T., Fellin, W., Kofler, A.: Snow avalanche friction relation based on extended kinetic theory. Nat. Hazard. **16**(11), 2325–2345 (2016). https://doi.org/10.5194/nhess-16-2325-2016
20. Bartelt, P., Salm, B., Gruber, U.: Calculating dense-snow avalanche runout using a Voellmy-fluid model with active/passive longitudinal straining. J. Glaciol. **45**(150), 242–254 (1999). https://doi.org/10.3189/S002214300000174X
21. Acheson, D.J.: Instability. Elementary Fluid Mechanics (Oxford University Press, 1990).
22. Bartelt, P., Bühler, Y., Buser, O., Christen, M., Meier, L.: Modeling mass-dependent flow regime transitions to predict the stopping and depositional behavior of snow avalanches. J. Geophys. Res. Earth Surf. (2012). https://doi.org/10.1029/2010JF001957
23. Iverson, R.M., Logan, M., LaHusen, R.G., Berti, M.: The perfect debris flow? Aggregated results from 28 large-scale experiments. J. Geophys. Res. Earth Surf. (2010). https://doi.org/10.1029/2009JF001514
24. Platzer, K., Bartelt, P., Kern, M.: Measurements of dense snow avalanche basal shear to normal stress ratios (S/N). Geophys. Res. Lett. (2007). https://doi.org/10.1029/2006GL028670
25. Liu, Y., Wang, H., Chen, H.Y., Hu, K.H., Wang, X.K.: The properties of dilute debris flow and hyper-concentrated flow in different flow regimes in open channels. J. Mt. Sci. **14**, 1728 (2017). https://doi.org/10.1007/s11629-016-4132-y
26. Takahashi, T.: Mechanical characteristics of debris flow. J. Hydraul. Div. **104**(8), 1153–1169 (1978)
27. Armanini, A., Capart, H., Fraccarollo, L., Larcher, M.: Rheological stratification in experimental free-surface flows of granular–liquid mixtures. J. Fluid Mech. **532**, 269–319 (2005). https://doi.org/10.1017/S0022112005004283
28. Cassar, C., Nicolas, M., Pouliquen, O.: Submarine granular flows down inclined planes. Phys. Fluids **17**(10), 103301 (2005). https://doi.org/10.1063/1.2069864
29. Kaitna, R., Dietrich, W.E., Hsu, L.: Surface slopes, velocity profiles and fluid pressure in coarse-grained debris flows saturated with water and mud. J. Fluid Mech. **741**, 377 (2014). https://doi.org/10.1017/jfm.2013.675
30. Johnson, C.G., Kokelaar, B.P., Iverson, R.M., Logan, M., LaHusen, R.G., Gray, J.M.N.T.: Grain-size segregation and levee formation in geophysical mass flows. J. Geophys. Res. Earth Surf. (2012). https://doi.org/10.1029/2011JF002185
31. Kokelaar, B.P., Graham, R.L., Gray, J.M.N.T., Vallance, J.W.: Fine-grained linings of leveed channels facilitate runout of granular flows. Earth Planet. Sci. Lett. **385**, 172–180 (2014). https://doi.org/10.1016/j.epsl.2013.10.043
32. Iverson, R.M.: The physics of debris flows. Rev. Geophys. **35**(3), 245–296 (1997). https://doi.org/10.1029/97RG00426
33. Berzi, D., Larcan, E.: Flow resistance of inertial debris flows. J. Hydraul. Eng. **139**(2), 187–194 (2012). https://doi.org/10.1061/(ASCE)HY.1943-7900.0000664
34. Iverson, R.M.: Mechanics of debris flows and rock avalanches. In: Fernando, H.J.S. (ed.) Handbook of Environmental Fluid Dynamics, vol. 1, pp. 573–587. CRC Press Taylor Francis (2013)
35. Rickenmann, D., Weber, D., Stepanov, B.: Erosion by debris flows in field and laboratory experiments. Debris-flow hazards mitigation: mechanics, prediction, and assessment, 883–894 (2003)
36. Jenkins, J.T., Zhang, C.: Kinetic theory for identical, frictional, nearly elastic spheres. Phys. Fluids **14**, 1228–1235 (2002). https://doi.org/10.1063/1.1449466
37. Bartelt, P., Buser, O.: The relation between dilatancy, effective stress and dispersive pressure in granular avalanches. Acta Geotech. **11**(3), 549–557 (2016). https://doi.org/10.1007/s11440-016-0463-7
38. Bartelt, P., Buser, O.: Reply to "Discussion of "The relation between dilatancy, effective stress and dispersive pressure in granular avalanches" by P. Bartelt and O. Buser. Acta Geotech. **11**(6), 1469–1473 (2016). https://doi.org/10.1007/s11440-016-0503-3
39. Bagnold, R.A.: Experiments on a gravity-free dispersion of large solid spheres in a Newtonian fluid under shear. Proc. R. Soc. A **225**, 49–63 (1954). https://doi.org/10.1098/rspa.1954.0186
40. Pitman, E.B., Le, L.: A two-fluid model for avalanche and debris flows. Philos. Trans. R. Soc. A Math. Phys. Eng. Sci. **363**(1832), 1573–1601 (2005). https://doi.org/10.1098/rsta.2005.1596
41. Baumgarten, A.S., Kamrin, K.: A general fluid–sediment mixture model and constitutive theory validated in many flow regimes. J. Fluid Mech. **861**, 721–764 (2019). https://doi.org/10.1017/jfm.2018.914